Supporting Information for

Decoding Proton-Coupled Electron Transfers with Non-Aqueous Potential-pK_a Diagrams

Brian D. McCarthy[1] and Jillian L. Dempsey[1]*

[1]Department of Chemistry, University of North Carolina, Chapel Hill, North Carolina 27599-3290, USA. E-mail: dempseyj@email.unc.edu

A. General experimental methods

General Considerations. Acetonitrile (Fisher Scientific, HPLC grade, >99.9%) and diethyl ether (Fisher Scientific, >99%) were dried and degassed with argon using a Pure Process Technology solvent system. *p*-Toluenesulfonic acid monohydrate (Sigma-Aldrich, ≥98.5%), tetraethylammonium *p*-toluenesulfonate (TCI America, >98%), decamethylferrocene (Acros Organics), benzoic acid (Aldrich, 99%), 2,4,6-tribromophenol (Sigma-Aldrich, 99%), 4-methoxypyridine (TCI America, >98%), 2-aminopyridine (TCI America, >99%), 2,4,6-trimethylpyridine (TCI America >98%), 2,3-diaminopyridine (Acros Organics, 98%), 2-aminobenzimidazole (Sigma-Aldrich, 97%), pentabromophenol (Sigma-Aldrich, 96%), and 4-dimethylaminopyridine (Alfa Aesar, 99%) were used as received. Tetrabutylammonium hexafluorophosphate (Acros Organics, 98%) was recrystallized from hot ethanol (Decon Labs, Inc., 200 proof), filtered, washed with cold ethanol, and dried at ca. 80 °C for about nine hours. 4-Bromoanilinium tetrafluoroborate, 4-chloroanilinium tetrafluoroborate, 4-tert-butylanilinium tetrafluoroborate, 4-methoxyanilinium tetrafluoroborate, and anilinium tetrafluoroborate were prepared as reported.[1] 4-Trifluoromethylanilinium tetrafluoroborate,[2] triethylammonium tetrafluoroborate,[3] [Ni(bdt)$_2$](Bu$_4$N),[4] and MoCp$_2$(S$_2$C$_2$(H)-4-pyridin-yl)[5] (MoCp$_2$(4-pedt)) were prepared by literature methods.

Trifluoroacetic acid (Sigma-Aldrich, 99%), 2,3,5,6-tetrafluoro-4-(trifluoromethyl)phenol (Sigma-Aldrich, 95%), 2,6-lutidine (Aldrich, 99+%), aniline (Sigma-Aldrich), 4-Cl-aniline (Aldrich, 98%), benzylamine (Acros, 99%), pyridine (Sigma-Aldrich, >99%), 2-methylpyridine (Alfa Aesar, 98+%), tetrafluoroboric acid diethyl ether complex (Aldrich), and 2,4,6-trimethylpyridine (TCI America, >98%) were degassed with three freeze-pump-thaw cycles. 2-Methylpyridine and pyridine were further dried over activated 3 Å molecular sieves. Deuterated acetonitrile (Cambridge Isotopes, 99.8%) was dried over activated 3 Å molecular sieves.

NMR spectra were taken with either a Bruker 400, 500, or 600 MHz spectrometer and were referenced to proteo solvent impurities.[6]

Electrochemical Methods. Electrochemistry was performed in a nitrogen-filled glovebox with a Pine Instruments WaveDriver potentiostat using glassy carbon working electrodes, a glassy carbon counter electrode, and a silver wire pseudoreference. The WaveDriver potentiostat was located outside the glovebox and a custom shielded electrode cable fed through a glovebox port. All scans are referenced vs. the ferrocene/ferrocenium couple. As an oxidation of compound **1** overlapped with the ferrocene/ferrocenium wave in some experiments, decamethylferrocene (-0.505 V vs. Fc$^{+/0}$) was used as an internal reference for experiments with **1**. Glassy carbon disk electrodes (CH Instruments, 3 mm diameter) were polished with Milli-Q water slurries of 0.05 micron alumina powder (CH Instruments, contained no agglomerating agents), rinsed, and ultrasonicated in Milli-Q water followed by rinsing with acetone and air drying. The pseudoreference silver wire electrode was submerged in a glass tube fitted with a porous glass Vycor tip containing 0.25 M [Bu$_4$N][PF$_6$].

Each working electrode was pretreated (two scans from about +0.7 V to –2.8 V) at 200 or 500 mV/s in 0.25 M [Bu$_4$N][PF$_6$] CH$_3$CN solution. The solution was agitated between CV experiments. Fresh electrodes were used for each measurement of [Ni(bdt)$_2$]$^−$ or MoCp$_2$(4-pedt) with different acids. For titration experiments of base to

solutions of MoCp₂(4-pedt) with acid it was found that the same electrode could be used for each CV without detriment.

Acid Syntheses

2,6-Dimethylpyridinium tetrafluoroborate was prepared by dissolving 2,6-dimethylpryidine (1 g) in ca. 5 mL Et$_2$O in a nitrogen-filled glovebox and tetrafluoroboric acid diethyl ether complex (0.95 mol. eq.) added in a dropwise manner, effecting rapid precipitation of the desired tetrafluoroborate salt. After removal of the diethyl ether under vacuum, the solids were dissolved in ca. 3 mL acetonitrile and reprecipitated by pouring into diethyl ether, following by decanting the solution, rinsing the solids with diethyl ether, and drying the remaining solids under vacuum for about one hour. Yield: 1.163 g, 67%. ^{1}H NMR (CD$_3$CN, ppm): 12.74 (broad s, 1 H), 8.28 (t, 1 H), 7.63 (d, 2 H), 2.70 (s, 6 H). Anal Calcd: C, 43.12; H, 5.17. Found: C, 43.13; H, 5.28.

Pyridinium tetrafluoroborate was prepared by dissolving in a nitrogen-filled glovebox 0.5 g of pyridine in ca. 10 mL Et$_2$O followed by portionwise addition of 0.9724 g of HBF$_4$-Et$_2$O (0.95 mol. eq.) with vigorous agitation. This effected precipitation of white solids; 5 mL more Et$_2$O was added and the supernatant decanted. The solids were washed five times with ca. 10 mL Et$_2$O each time followed by drying under vacuum at room temperature for about 5 hours. Yield: 0.81 g, 81%. ^{1}H NMR (CD$_3$CN, ppm): 13.09 (broad s, 1 H), 8.71 (d, 2 H), 8.62 (t, 1 H), 8.06 (m, 2 H). Anal Calcd: C, 35.98; H, 3.62. Found: C, 35.75; 3.66.

2-Methylpyridinium tetrafluoroborate was prepared by dissolving 1 g of 2-methylpyridine in ca. 4 mL CH$_3$CN followed by dropwise addition of 1.652 g HBF$_4$-Et$_2$O complex (0.95 mol. eq.). Addition of ca. 10 mL of Et$_2$O effected separation of a dense oil. The supernatant was decanted and the oil vigorously washed twice with 10 mL Et$_2$O followed by drying under vacuum at ca. 60 °C for twenty minutes to yield a viscous liquid. Yield: 1.27 g, 69%. ^{1}H NMR (CD$_3$CN, ppm): 12.42 (broad s, 1 H), 8.54 – 8.45 (two multiplets, 2 H), 7.85 (m, 2 H), 2.75 (m, 3 H). Anal Calcd: C, 39.83; H, 4.46. Found: C, 39.31; H, 4.48.

2-Aminopyridinium tetrafluoroborate was synthesized as for 2-methylpyridinium with 1 g of 2-aminopyridine and 1.635 g HBF$_4$-Et$_2$O (0.95 mol. eq.). As for 2-methylpyridinium, an oil initially formed after Et$_2$O addition; however, during the second Et$_2$O wash waxy white solids precipitated; these were dried under vacuum at about 60 °C for twenty minutes. Yield: 1.2 g, 65%. ^{1}H NMR (CD$_3$CN, ppm): 10.71 (broad s, 1 H), 7.89 (mm, 1 H), 7.78 (d, 1 H), 7.02 (d, 1 H), 6.88 (t, 1 H), 6.62 (broad s, 2 H). Anal Calcd: C, 33.01; H, 3.88. Found: C, 33.09; H, 4.01.

4-Methoxypyridinium tetrafluoroborate was prepared as for 2-aminopyridinium. The waxy solids isolated after the second Et$_2$O wash were briefly dried under vacuum followed by dissolution in a minimal amount of acetone. Diethyl ether was added dropwise until the solution became cloudy; acetone was then added until the solution became clear again. This solution was cooled at about -40 °C overnight to yield blocky white crystals. The crystals were crushed, washed twice with 10 mL Et$_2$O, and dried under vacuum at ca. 60 °C for twenty minutes. Yield: 0.12 g, 7%. ^{1}H NMR (CD$_3$CN, ppm): 12.10 (broad s, 1 H), 8.48 (d, 2 H), 7.41 (d, 2 H), 4.09 (s, 3 H). Anal Calcd: C, 33.01; H, 3.88. Found: C, 36.50; H, 4.10.

2,4,6-Trimethylpyridinium tetrafluoroborate was prepared by dissolving 1 g of 2,4,6-trimethylpyridine in ca. 5 mL Et$_2$O followed by dropwise addition with stirring of 1.17

g of HBF$_4$-Et$_2$O (0.95 mol. eq.), effecting precipitation of white solids. The solvent was removed under vacuum. The solids were dissolved in a minimal amount of CH$_3$CN and Et$_2$O added until solids precipitated. After decanting, the solids were washed three times with ca. 15 mL Et$_2$O followed by drying under vacuum at ca. 60 °C for 30 minutes. Yield: 1.2 g, 73%. ^{1}H NMR (CD$_3$CN, ppm): 11.48 (broad s, 1 H), 7.42 (s, 2 H), 2.62 (s, 6 H), 2.51 (s, 3 H). Anal Calcd: C, 45.98; H, 5.79. Found: C, 46.25; H, 5.96.

2-Aminobenzimidazolium tetrafluoroborate was prepared by suspending 1 g of 2-aminobenzimidazole in ca. 5 mL Et$_2$O followed by dropwise addition with stirring of 1.155 g of HBF$_4$-Et$_2$O (0.95 mol. eq.) with 2 mL Et$_2$O, effecting precipitation of white solids. The reaction vial was capped and shaken vigorously to ensure adequate mixing. The solvent was removed under vacuum. The solids were dissolved in a minimal amount of CH$_3$CN and Et$_2$O added until solids precipitated. After decanting, the solids were washed three times with ca. 15 mL Et$_2$O followed by drying under vacuum at ca. 60 °C for 30 minutes. Yield: 0.35 g, 22%. ^{1}H NMR (CD$_3$CN, ppm): 10.03 (broad s, 2 H), 7.45 – 7.42 (m, 2 H), 7.30 – 7.28 (m, 2H), 6.81 (broad s, 2 H). Anal Calcd: C, 38.05; H, 3.65. Found: C, 38.17; H, 3.67.

Table S1. Summary of acids used and synthetic sources.

acid	pK_a (ref.)	synthesis ref.
dimethylformamidium triflate	6.1 (7)	1
4-cyanoanilinium tetrafluoroborate	7 (8)	1
4-trifluoromethylaminilinium tetrafluoroborate	8.03 (9)	2
p-toluenesulfonic acid monohydrate	8.6 (10)	*commercial*
4-(methylbenzoate)anilinium tetrafluoroborate	8.62 (2)	2
4-trifluoromethoxyanilinium tetrafluoroborate	9.28 (2)	2
4-bromoanilinium tetrafluoroborate	9.43 (9)	1
4-chloroanilinium tetrafluoroborate	9.7 (1)	1
anilinium tetrafluoroborate	10.62 (9)	1
4-tertbutylanilinium tetrafluoroborate	11.1 (1)	1
4-methylanilinium tetrafluoroborate	11.4 (11)	11
N,N-dimethylanilinium tetrafluoroborate	11.43 (9)	1
4-methoxyanilinium tetrafluoroborate	11.86 (9)	1
pyridinium tetrafluoroborate	12.53 (9)	this work
trifluoroacetic acid	12.65 (7)	*commercial*
2-methylpyridinium tetrafluoroborate	13.32 (9)	this work
2,6-dimethylpyridinium tetrafluoroborate	14.13 (9)	this work
4-methoxypyridinium tetrafluoroborate	14.23 (9)	this work
2-aminopyridinium tetrafluoroborate	14.47 (9)	this work
2,4,6-trimethylpyridinium tetrafluoroborate	14.98 (9)	this work
2-aminobenzimidazolium tetrafluoroborate	16.08 (9)	this work
4-trifluoromethyl-2,3,5,6-tetrafluorophenol	16.62 (10)	*commercial*
pentabromophenol	17.83 (10)	*commercial*
triethylammonium tetrafluoroborate	18.82 (10)	this work
2,4,6-tribromophenol	20.35 (10)	*commercial*
benzoic acid	21.51 (10)	*commercial*

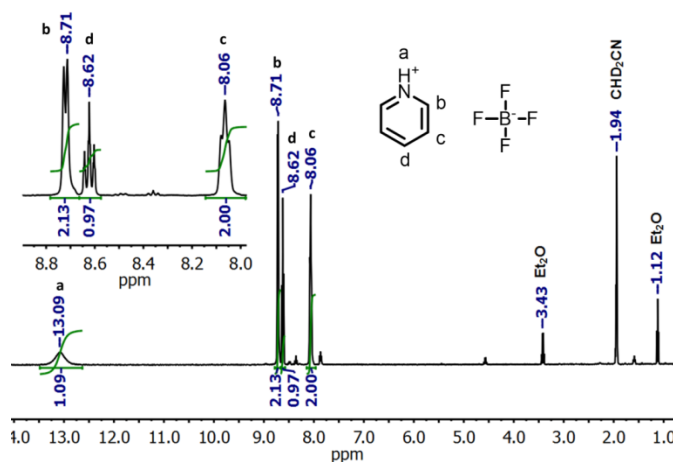## B. ¹H NMR spectra of acids in anhydrous CD₃CN

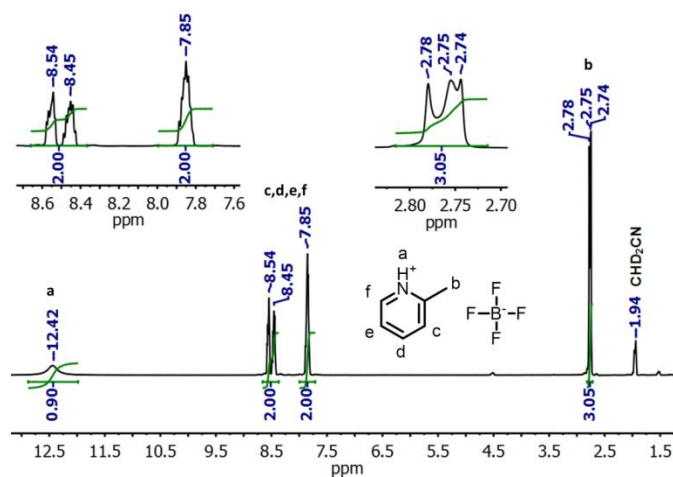**Figure SB1.** ¹H NMR of pyridinium tetrafluoroborate in CD₃CN.

Figure SB2. ¹H NMR of 2-methylpyridinium tetrafluoroborate in CD₃CN.
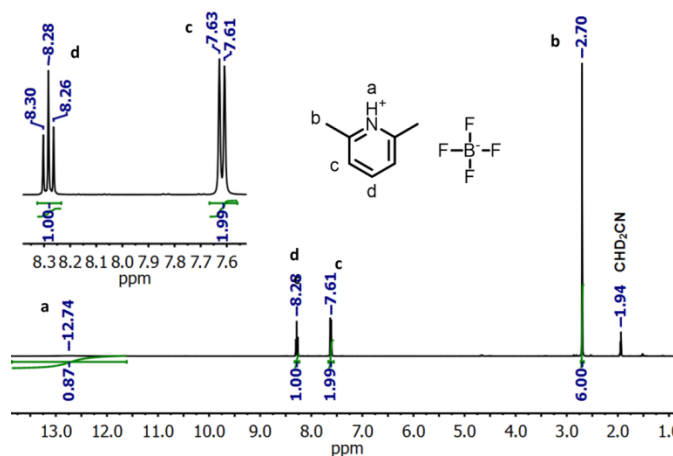

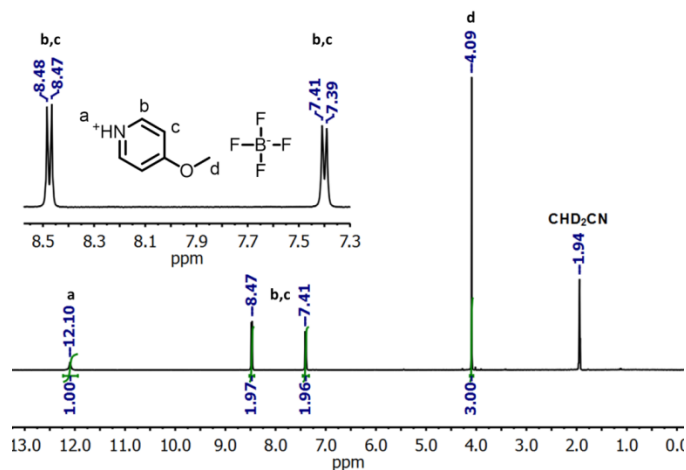**Figure SB3.** ¹H NMR of 2,6-lutidinium tetrafluoroborate in CD₃CN.

5

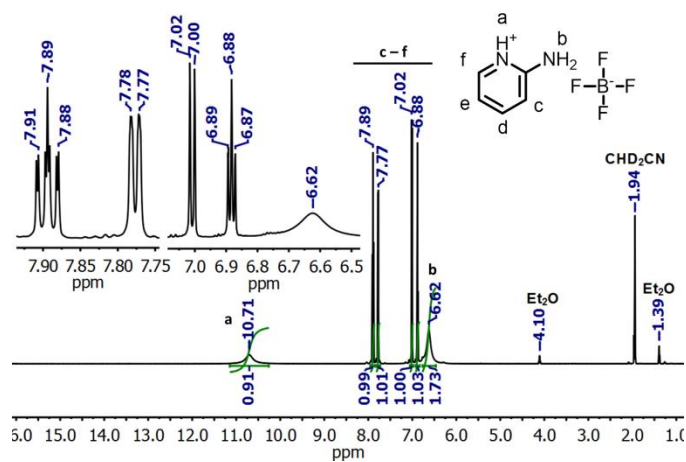**Figure SB4.** ^{1}H NMR of 4-methoxypyridinium tetrafluoroborate in CD$_3$CN.

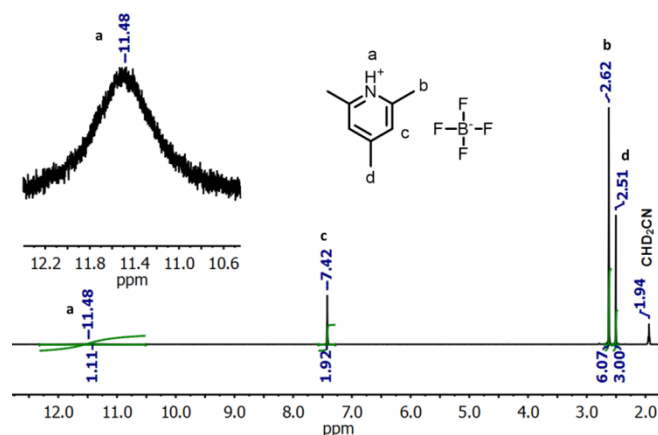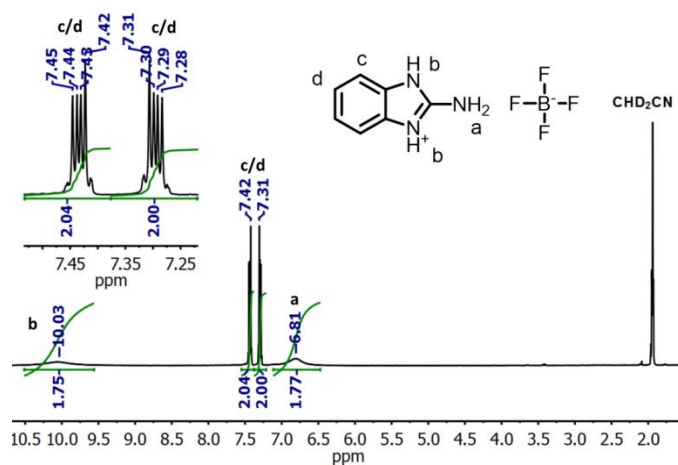**Figure SB5.** ^{1}H NMR of 2-aminopyridinium tetrafluoroborate in CD$_3$CN.

Figure SB6. ^{1}H NMR of 2,4,6-trimethylpyridinium tetrafluoroborate in CD$_3$CN.

Figure SB7. ^{1}H NMR of 2-aminobenzimidazolium tetrafluoroborate in CD$_3$CN.

C. Cyclic voltammetry data for PCET reaction of 1 and acids

Table SC1. Summary of acids used for electrochemical PCET with **1** and observed $E_{1/2}$.

acid	$pK_a(CH_3CN)$	$E_{1/2}$ for **1** + acid (V)
dimethylformamidium triflate	6.1	0.005
4-cyanoanilinium tetrafluoroborate	7	0.009
4-trifluoromethylaminilinium tetrafluoroborate	8.03	0.008
p-toluenesulfonic acid monohydrate	8.6	0.005
4-(methylbenzoate)anilinium tetrafluoroborate	8.62	0.004
4-trifluoromethoxyanilinium tetrafluoroborate	9.28	0.008
4-bromoanilinium tetrafluoroborate	9.43	0.005
4-chloroanilinium tetrafluoroborate	9.7	0.005
anilinium tetrafluoroborate	10.62	-0.003
4-tertbutylanilinium tetrafluoroborate	11.1	-0.005
4-methylanilinium tetrafluoroborate	11.4	-0.010
N,N-dimethylanilinium tetrafluoroborate	11.43	-0.010
4-methoxyanilinium tetrafluoroborate	11.86	-0.015
pyridinium tetrafluoroborate	12.53	-0.058
trifluoroacetic acid	12.65	-0.044
2-methylpyridinium tetrafluoroborate	13.32	-0.088
2,6-dimethylpyridinium tetrafluoroborate	14.13	-0.130
4-methoxypyridinium tetrafluoroborate	14.23	-0.137
2-aminopyridinium tetrafluoroborate	14.47	-0.160
2,4,6-trimethylpyridinium tetrafluoroborate	14.98	-0.162
2-aminobenzimidazolium tetrafluoroborate	16.08	-0.193
4-trifluoromethyl-2,3,5,6-tetrafluorophenol	16.62	-0.185
pentabromophenol	17.83	-0.195
triethylammonium tetrafluoroborate	18.82	-0.205
2,4,6-tribromophenol	20.35	-0.205
benzoic acid	21.51	-0.202

Cyclic voltammograms – in each case decamethylferrocene is present as an internal reference (-0.505 V vs. $Fc^{+/0}$ as measured in our lab). Varying amounts of internal standard were used from experiment to experiment; it was used solely as a reference for the applied potential. The amount of acid and **1** were carefully controlled through the use of fresh stock solutions containing pure materials.
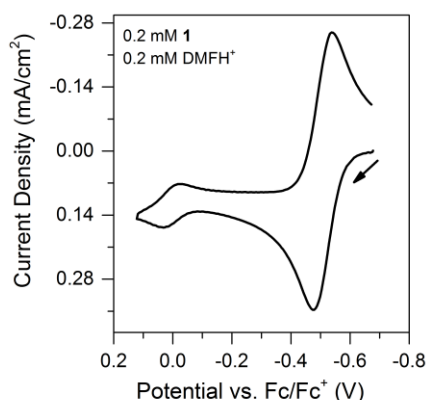

Figure SC1. Cyclic voltammogram of 0.2 mM **1**, 0.2 mM dimethylformamidium triflate, and decamethylferrocene in 0.25 M [Bu₄N][PF₆] CH₃CN solution at 100 mV/s.
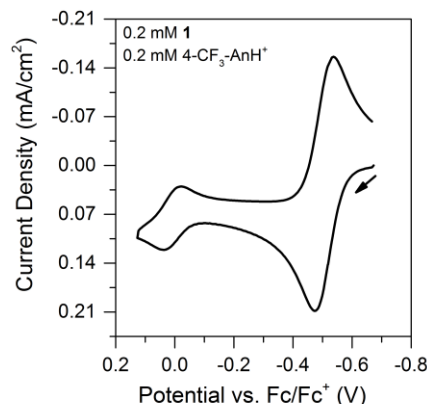
Figure SC3. Cyclic voltammogram of 0.2 mM **1**, 0.2 mM 4-trifluoromethylanilinium tetrafluoroborate, and decamethylferrocene in 0.25 M [Bu₄N][PF₆] CH₃CN solution at 100 mV/s.
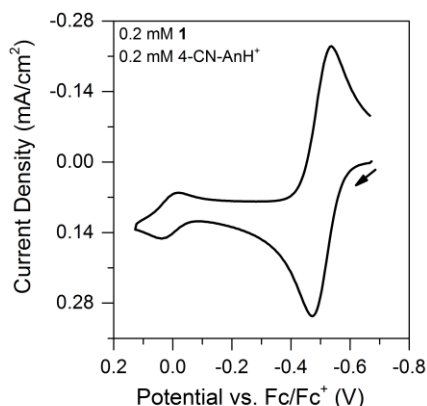
Figure SC2. Cyclic voltammogram of 0.2 mM **1**, 0.2 mM 4-cyanoanilinium tetrafluoroborate, and decamethylferrocene in 0.25 M [Bu₄N][PF₆] CH₃CN solution at 100 mV/s.
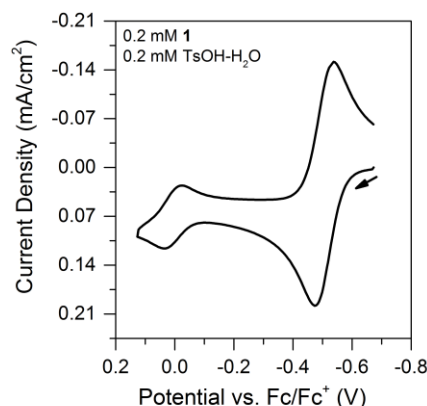
Figure SC4. Cyclic voltammogram of 0.2 mM **1**, 0.2 mM *p*-toluenesulfonic acid monohydrate, and decamethylferrocene in 0.25 M [Bu₄N][PF₆] CH₃CN solution at 100 mV/s.
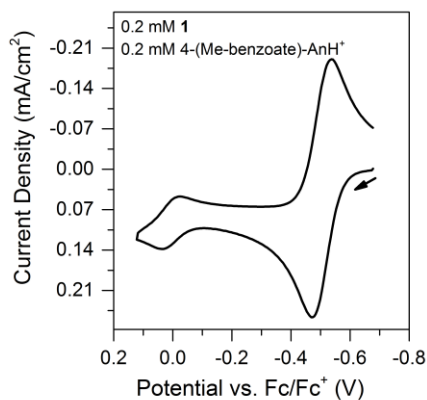
Figure SC5. Cyclic voltammogram of 0.2 mM **1**, 0.2 mM 4-(methylbenzoate)anilinium tetrafluoroborate, and decamethylferrocene in 0.25 M [Bu$_4$N][PF$_6$] CH$_3$CN solution at 100 mV/s.

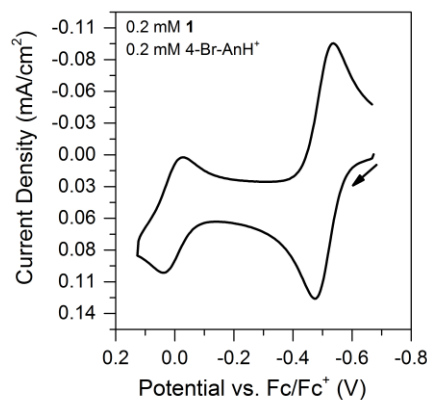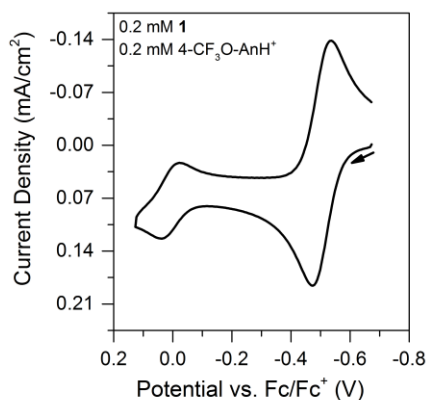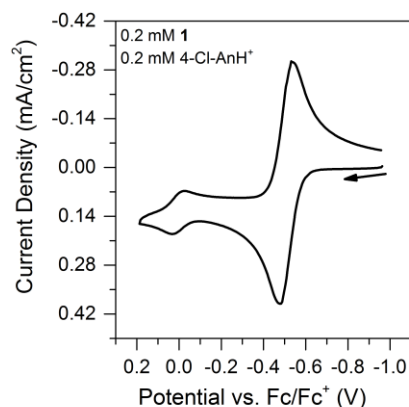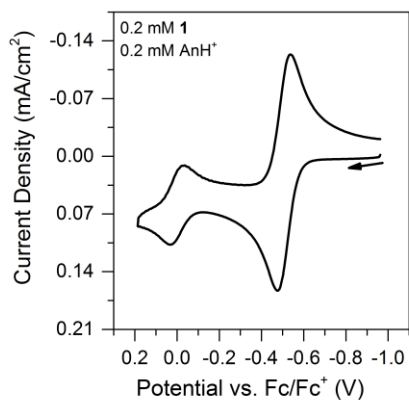**Figure SC7.** Cyclic voltammogram of 0.2 mM **1**, 0.2 mM 4-bromoanilinium tetrafluoroborate, and decamethylferrocene in 0.25 M [Bu$_4$N][PF$_6$] CH$_3$CN solution at 100 mV/s.

Figure SC6. Cyclic voltammogram of 0.2 mM **1**, 0.2 mM 4-trifluoromethoxyanilinium tetrafluoroborate, and decamethylferrocene in 0.25 M [Bu$_4$N][PF$_6$] CH$_3$CN solution at 100 mV/s.
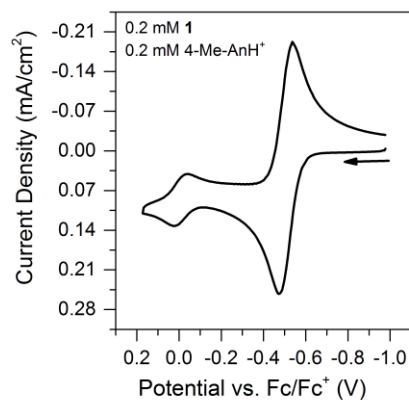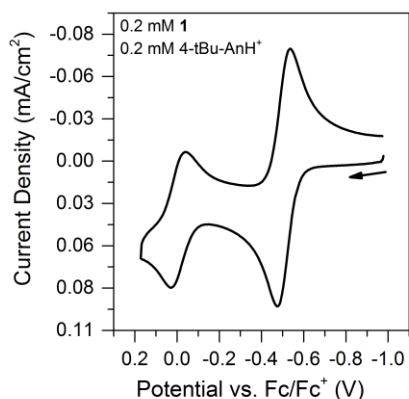

Figure SC8. Cyclic voltammogram of 0.2 mM **1**, 0.2 mM 4-chloroanilinium tetrafluoroborate, and decamethylferrocene in 0.25 M [Bu$_4$N][PF$_6$] CH$_3$CN solution at 100 mV/s.

10

Figure SC9. Cyclic voltammogram of 0.2 mM **1**, 0.2 mM anilinium tetrafluoroborate, and decamethylferrocene in 0.25 M [Bu₄N][PF₆] CH₃CN solution at 100 mV/s.

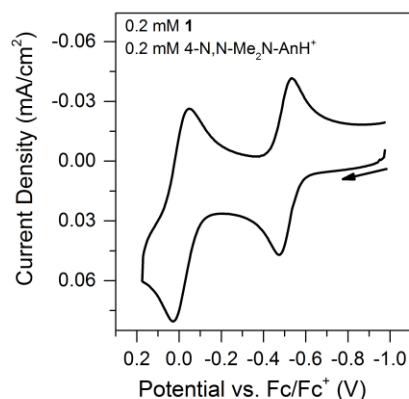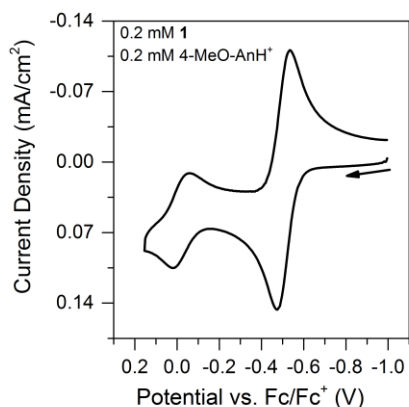**Figure SC11.** Cyclic voltammogram of 0.2 mM **1**, 0.2 mM 4-methylanilinium tetrafluoroborate, and decamethylferrocene in 0.25 M [Bu₄N][PF₆] CH₃CN solution at 100 mV/s.

Figure SC10. Cyclic voltammogram of 0.2 mM **1**, 0.2 mM 4-tertbutylanilinium tetrafluoroborate, and decamethylferrocene in 0.25 M [Bu₄N][PF₆] CH₃CN solution at 100 mV/s.

Figure SC12. Cyclic voltammogram of 0.2 mM **1**, 0.2 mM *N,N*-dimethylanilinium tetrafluoroborate, and decamethylferrocene in 0.25 M [Bu₄N][PF₆] CH₃CN solution at 100 mV/s.

11

Figure SC13. Cyclic voltammogram of 0.2 mM **1**, 0.2 mM 4-methoxyanilinium tetrafluoroborate, and decamethylferrocene in 0.25 M [Bu₄N][PF₆] CH₃CN solution at 100 mV/s.
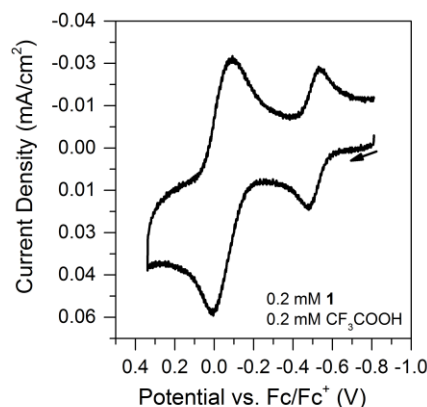

Figure SC15. Cyclic voltammogram of 0.2 mM **1**, 0.2 mM trifluoroacetic acid, and decamethylferrocene in 0.25 M [Bu₄N][PF₆] CH₃CN solution at 100 mV/s.
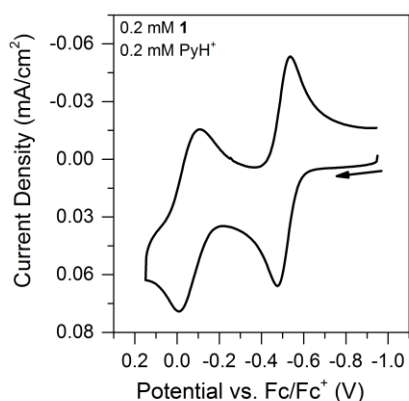

Figure SC14. Cyclic voltammogram of 0.2 mM **1**, 0.2 mM pyridinium tetrafluoroborate, and decamethylferrocene in 0.25 M [Bu₄N][PF₆] CH₃CN solution at 100 mV/s.

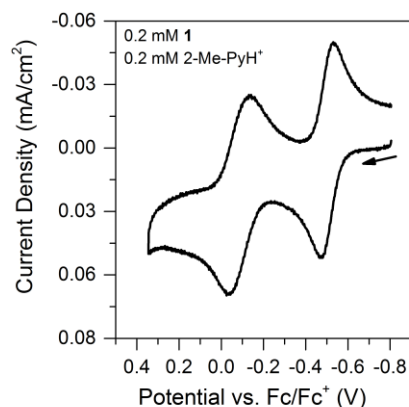**Figure SC16.** Cyclic voltammogram of 0.2 mM **1**, 0.2 mM 2-methylpyridinium tetrafluoroborate, and decamethylferrocene in 0.25 M [Bu₄N][PF₆] CH₃CN solution at 100 mV/s.
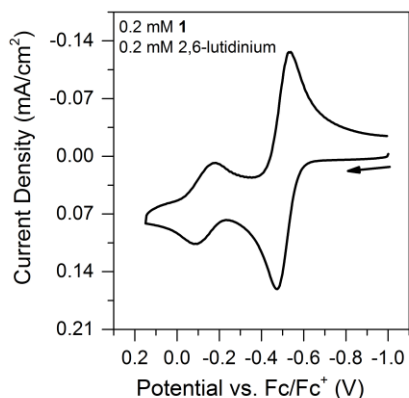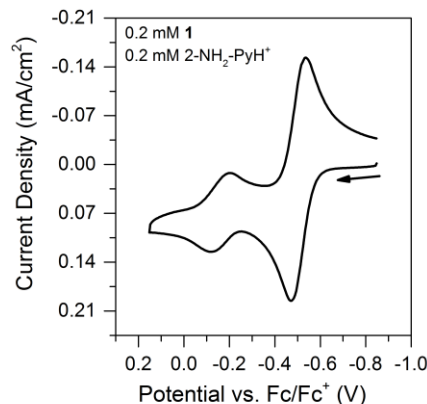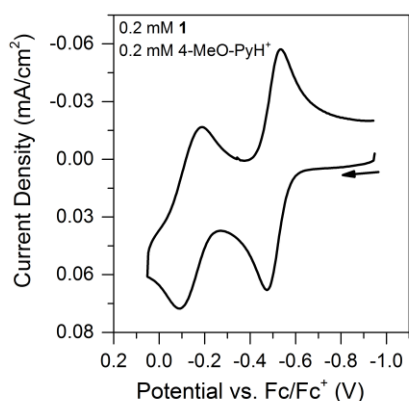
Figure SC17. Cyclic voltammogram of 0.2 mM **1**, 0.2 mM 2,6-lutidinium tetrafluoroborate, and decamethylferrocene in 0.25 M [Bu$_4$N][PF$_6$] CH$_3$CN solution at 100 mV/s.

Figure SC19. Cyclic voltammogram of 0.2 mM **1**, 0.2 mM 2-aminopyridinium tetrafluoroborate, and decamethylferrocene in 0.25 M [Bu$_4$N][PF$_6$] CH$_3$CN solution at 100 mV/s.

Figure SC18. Cyclic voltammogram of 0.2 mM **1**, 0.2 mM 4-methoxypyridinium tetrafluoroborate, and decamethylferrocene in 0.25 M [Bu$_4$N][PF$_6$] CH$_3$CN solution at 100 mV/s.
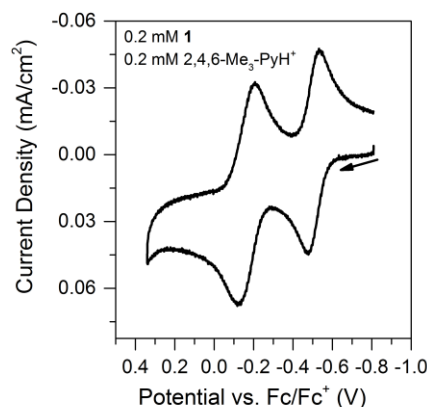

Figure SC20. Cyclic voltammogram of 0.2 mM **1**, 0.2 mM 2,4,6-trimethylpyridinium tetrafluoroborate, and decamethylferrocene in 0.25 M [Bu$_4$N][PF$_6$] CH$_3$CN solution at 100 mV/s.
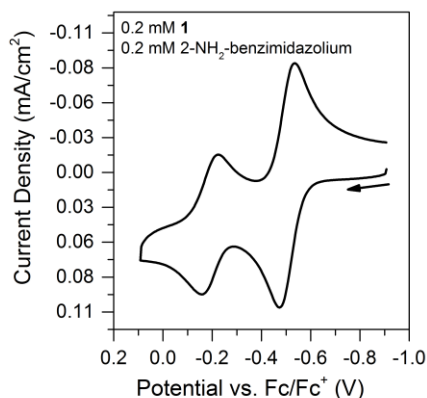
Figure SC21. Cyclic voltammogram of 0.2 mM **1**, 0.2 mM 2-aminobenzimidazolium tetrafluoroborate, and decamethylferrocene in 0.25 M [Bu$_4$N][PF$_6$] CH$_3$CN solution at 100 mV/s.

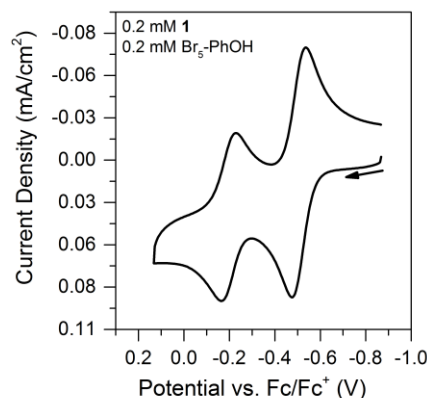**Figure SC23.** Cyclic voltammogram of 0.2 mM **1**, 0.2 mM pentabromophenol, and decamethylferrocene in 0.25 M [Bu$_4$N][PF$_6$] CH$_3$CN solution at 100 mV/s.

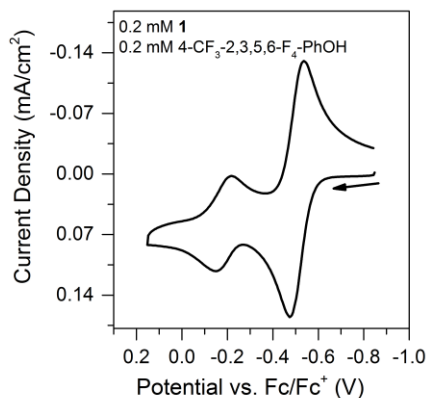**Figure SC22.** Cyclic voltammogram of 0.2 mM **1**, 0.2 mM 4-trifluoromethyl-2,3,5,6-tetrafluorophenol, and decamethylferrocene in 0.25 M [Bu$_4$N][PF$_6$] CH$_3$CN solution at 100 mV/s.
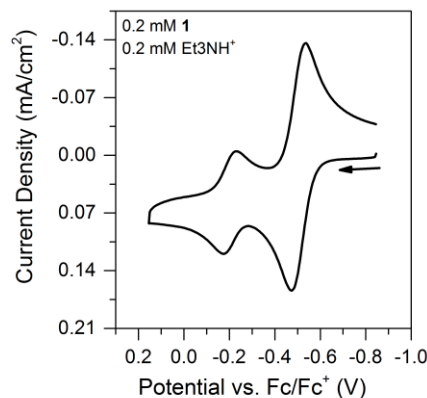
Figure SC24. Cyclic voltammogram of 0.2 mM **1**, 0.2 mM triethylammonium tetrafluoroborate, and decamethylferrocene in 0.25 M [Bu$_4$N][PF$_6$] CH$_3$CN solution at 100 mV/s.

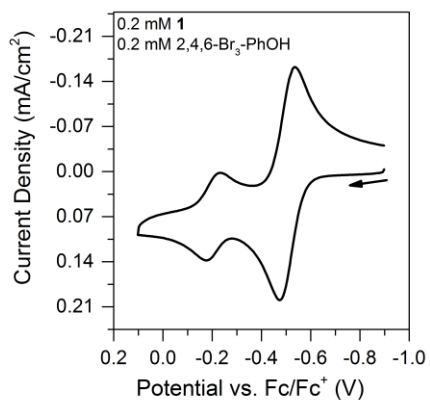**Figure SC25.** Cyclic voltammogram of 0.2 mM **1**, 0.2 mM 2,4,6-tribromophenol, and decamethylferrocene in 0.25 M [Bu₄N][PF₆] CH₃CN solution at 100 mV/s.

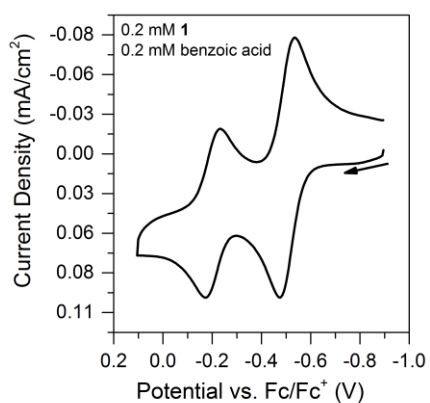**Figure SC26.** Cyclic voltammogram of 0.2 mM **1**, 0.2 mM benzoic acid, and decamethylferrocene in 0.25 M [Bu₄N][PF₆] CH₃CN solution at 100 mV/s.

D. Modeling PCET of 1 with acids as stepwise ET-PT or PT-ET mechanisms

Thermochemistry of an EC Reaction Mechanism

    In an EC reaction mechanism, electron transfer at the electrode is coupled to a follow-up first-order (or pseudo first-order) homogeneous reaction. The EC reaction scheme for **[1(H)]$^{1+}$** is depicted in Figure SD1, where the reversible oxidation of **[1(H)]$^{1+}$** yields an equilibrium mixture of **[1(H)]$^{2+}$** and **[1]$^{1+}$**:
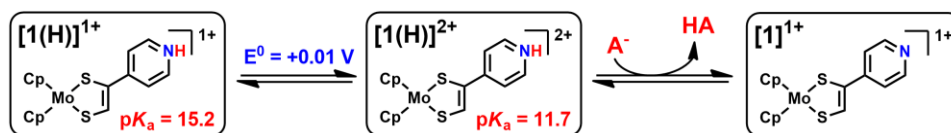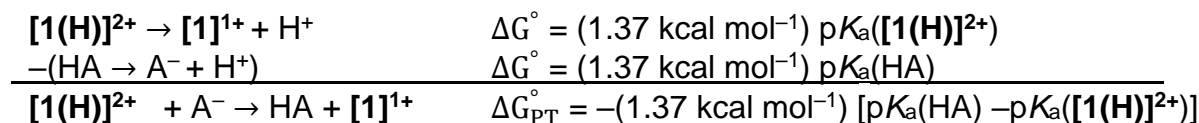

Figure SD1. EC mechanism for oxidation of **1**.

Under the conditions of fast electrode electron transfer (such that the homogeneous follow-up reaction and diffusion are rate limiting), the electrochemical response is a function of the equilibrium constant (K_{EC}) and the dimensionless parameter λ.[12]

$$K_{EC} = k_+/k_-$$

$$\lambda = \frac{RT}{F}\frac{k_+ + k_-}{v} = \frac{RT}{F}\frac{k}{v}$$

The equilibrium constant K_{EC} can be readily related to the free energy change associated with the deprotonation of **[1(H)]$^{2+}$** by the conjugate base of HA:[13]

[1(H)]$^{2+}$ → **[1]$^{1+}$** + H$^+$	ΔG° = (1.37 kcal mol^{-1}) pK_a(**[1(H)]$^{2+}$**)
−(HA → A$^-$ + H$^+$)	ΔG° = (1.37 kcal mol^{-1}) pK_a(HA)
[1(H)]$^{2+}$ + A$^-$ → HA + **[1]$^{1+}$**	ΔG°_{PT} = −(1.37 kcal mol^{-1}) [pK_a(HA) −pK_a(**[1(H)]$^{2+}$**)]

$$K_{EC} = e^{-\Delta G^\circ_{PT}/RT}$$

For a reversible chemical reaction following the *oxidation* of **[1(H)]$^{1+}$** to **[1(H)]$^{2+}$** (zone DE), a reversible Nernstian wave centered around a new formal potential ($E_{1/2}$) is anticipated, which is related to K_{EC} and $E^{o'}$ (the formal potential of the **[1(H)]$^{2+/1+}$** couple) by:[12,14]

$$E_{1/2} = E^{o'}([\mathbf{1(H)}]^{2+/1+}) - \frac{RT}{F}\ln(1 + K_{EC})$$

The new formal potential will appear at potentials *cathodic* to $E^{o'}$ for an oxidative process (Figure SD2).† At pK_a(HA) values < ca. 10, $E_{1/2} \approx E^o$. In the region 10 < pK_a(HA) < 13, the $E_{1/2}$–pK_a relationship has curvature. For pK_a(HA) values > ca. 13, a linear relationship between $E_{1/2}$ and pK_a(HA) is observed, with a slope of 59 mV/decade, consistent with the relationship predicted by Equation 12.

---

† The relationship between E$_{1/2}$ and K_{EC} has been derived for a *reductive* process (Ref. 12). In this case, E$_{1/2}$ appear at potentials anodic to E$^{0'}$ and the relationship is defined by $E_{1/2} = E^{0'} + \frac{RT}{F}\ln(1 + K_{EC})$. For an oxidative process, the sign should change and E$_{1/2}$ should appear cathodic of the oxidative wave defined by E$^{0'}$.
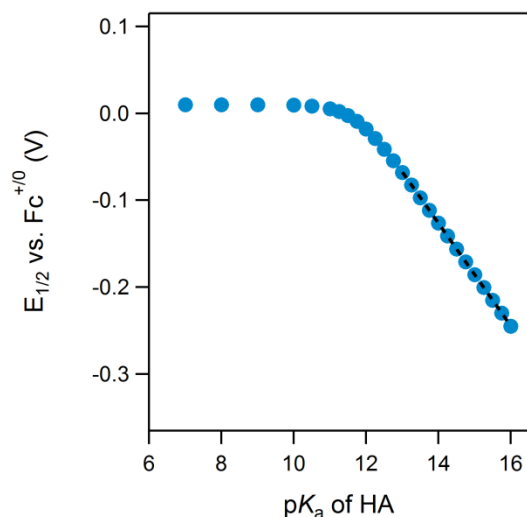
Figure SD2. The predicted relationship between $E_{1/2}$ and the pK_a of HA for an EC reaction (•) reveals a linear region (---) with a slope of 59 V/decade for pK_a values greater than ca. 13.

Thermochemistry of a CE Reaction Mechanism

In a CE reaction mechanism, a first-order (or pseudo first-order) homogeneous reaction is followed by an electron transfer at the electrode. The CE reaction scheme for **1** is depicted in Figure SD3, where **1** and **[1(H)]$^{1+}$** are in equilibrium and **1** can be oxidized to **[1]$^{1+}$**:
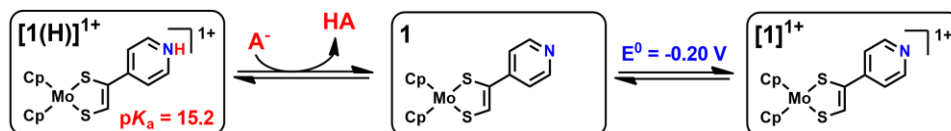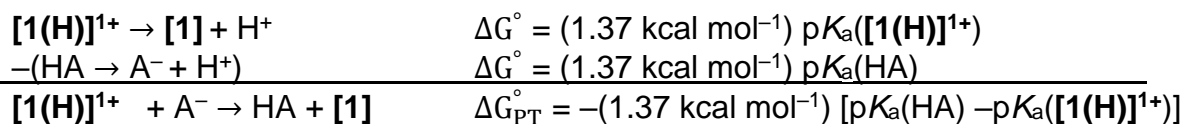

Figure SD3. CE mechanism for oxidation of **1**.

When electrode electron transfer is fast (such that the kinetics of the homogeneous reaction and diffusion are rate limiting), the electrochemical response is a function of the equilibrium constant (K_{CE}) and the dimensionless kinetic parameter λ.[12]

$$K_{CE} = k_+/k_-$$

$$\lambda = \frac{RT}{F}\frac{k_+ + k_-}{v} = \frac{RT}{F}\frac{k}{v}$$

The equilibrium constant K_{CE} can be readily related to the free energy change associated with the deprotonation of **[1(H)]$^{1+}$** by the conjugate base of HA:[13]

[1(H)]$^{1+}$ → [1] + H$^+$	ΔG° = (1.37 kcal mol^{-1}) pK_a(**[1(H)]$^{1+}$**)
−(HA → A$^-$ + H$^+$)	ΔG° = (1.37 kcal mol^{-1}) pK_a(HA)
[1(H)]$^{1+}$ + A$^-$ → HA + **[1]**	ΔG°_{PT} = −(1.37 kcal mol^{-1}) [pK_a(HA) −pK_a(**[1(H)]$^{1+}$**)]

$$K_{CE} = e^{-\Delta G^\circ_{PT}/RT}$$

17

In zone DE (large values of λ, small to moderate K_{CE}), a reversible Nernstian wave centered around a new formal potential ($E_{1/2}$), anodic to $E^{o\prime}([\mathbf{1}]^{+/\mathbf{0}})$, is expected.[‡] $E_{1/2}$ is related to K_{CE} and $E^{o\prime}([\mathbf{1}]^{+/\mathbf{0}})$ by:[12,14]

$$E_{1/2} = E^{o\prime}([\mathbf{1}]^{+/\mathbf{0}}) - \frac{RT}{F}\ln\left(\frac{K_{CE}}{1+K_{CE}}\right)$$

At pK_a values > ca. 16.5, $E_{1/2} \approx E^o$. In the region $16.5 < pK_a(HA) < 14.25$, the $E_{1/2}$–pK_a relationship has curvature. For $pK_a(HA)$ values < ca. 14.25, a linear relationship between $E_{1/2}$ and $pK_a(HA)$ is observed, with a slope of 59 mV/decade, consistent with the relationship predicted by Equation 12.
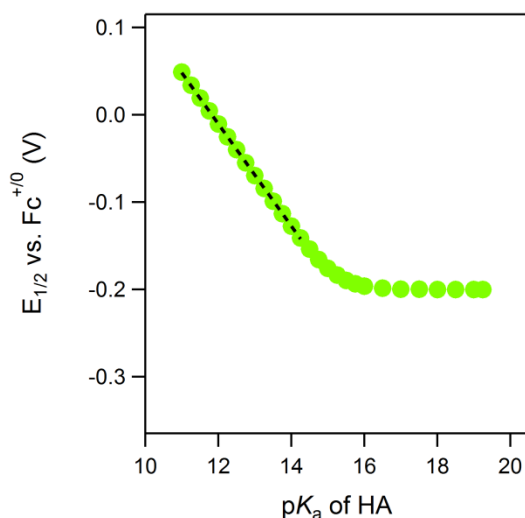

Figure SD4. The predicted relationship between $E_{1/2}$ and the pK_a of HA for a CE reaction (•) reveals a linear region (---) with a slope of 59 V/decade for pK_a values less than ca. 14.25.

Unifying EC and CE mechanisms

As demonstrated above, both of the EC and CE mechanisms predict a 59 mV/decade dependence of the observed redox wave on the acid pK_a. Both also predict curvature near the pK_a of **[1(H)]⁺** and **[1(H)]²⁺**. These results are consistent with the predicted slope of Eq. 12 (main text) and the curvature observed in the experimental potential-pK_a diagram of **1**. If the simulated peak shifts of the EC and CE mechanisms are overlaid on the same plot it is clear that it is a quantitative match for the experimental potential–pK_a diagram of **1** (Figure SD5). The observed curvature can be explained by the equilibrium that exists near the pK_a values of the two intermediates **[1(H)]⁺** and **[1(H)]²⁺**.

[‡] The relationship between $E_{1/2}$ and K_{CE} has been derived for a *reductive* process (Ref. 12). In this case, $E_{1/2}$ appear at potentials cathodic to $E^{0\prime}$ and the relationship is defined by $E_{1/2} = E^{o\prime} + \frac{RT}{F}\ln\left(\frac{K_{CE}}{1+K_{CE}}\right)$. For an oxidative process, the sign should change and $E_{1/2}$ should appear anodic of the oxidative wave defined by $E^{0\prime}$.
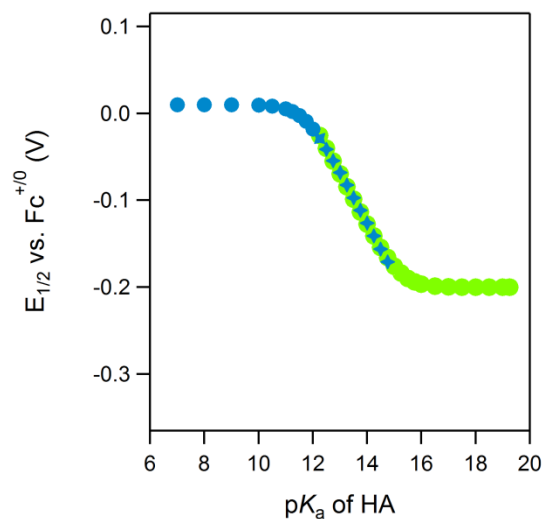
Figure SD5. Overlay of the predicted relationship between $E_{1/2}$ and the pK_a of HA for both the CE (•) and EC (•) mechanisms.

Thermochemically, the match between the EC and CE mechanisms as well as the adherence of the experimental data for **1** to Hess's law confirm that a thermochemical cycle can be made relating the two mechanisms. This also confirms that the concerted reaction (EC) is thermodynamically accessible. The overlapping predictions of the EC and CE simulated redox shift strongly hints that the mechanism is pK_a-dependent. The possibility of a concerted pathway at some pK_a values is also possible.

E. Cyclic voltammetry data for PCET reaction of 2 and acids

Table SE1. Summary of acids used for electrochemical PCET with **2** and average $E_{1/2}$ for PCET.

acid[a]	pK_a(CH$_3$CN)	ref. for pK_a	Avg. $E_{1/2}$ for **2** + acid (V)[b]
4-trifluoromethylanilinium	8.03	9	-0.681
p-toluenesulfonic acid	8.6	10	-0.725
4-bromoanilinium	9.43	9	-0.785
4-chloroanilinium	9.7	1	-0.794
anilinium	10.62	9	-0.85
4-tert-butylanilinium	11.1	1	-0.878
4-methoxyanilinium	11.86	9	-0.896
trifluoroacetic acid	12.65	7	-0.902
2,6-lutidinium	14.13	9	-0.918
2,4,6-trimethylpyridinium	14.98	9	-0.915
4-CF$_3$-2,3,5,6-F$_4$-PhOH	16.62	10	-0.916
triethylammonium	18.82	9	-0.915

[a]Unless otherwise stated, acids used had tetrafluoroborate counteranions. [b]Average of at least three CVs at different scan rates where both reduction and oxidation could be observed.
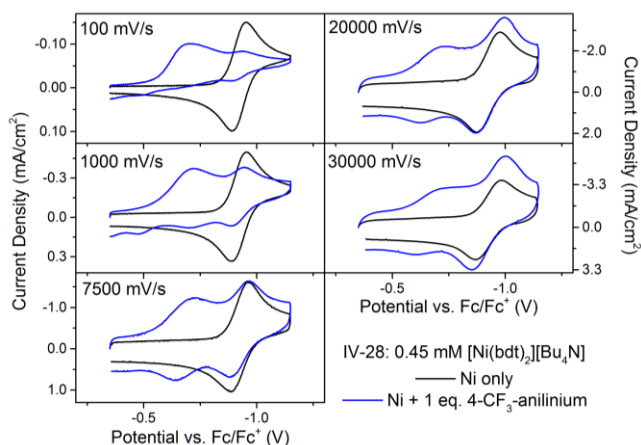

Figure SE1. Cyclic voltammograms of 0.45 mM **2** with and without one molar equivalent of 4-CF$_3$-anilinium, at varying scan rates. Recorded in 0.25 M [Bu$_4$N][PF$_6$] CH$_3$CN solution.
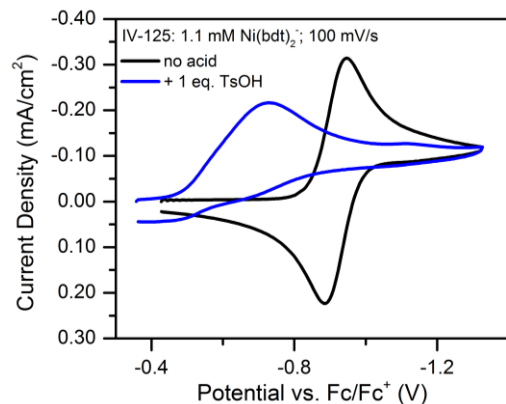
Figure SE2. Cyclic voltammograms of 0.45 mM **2** with and without one molar equivalent of *p*-toluenesulfonic acid at 100 mV/s. Recorded in 0.25 M [Bu$_4$N][PF$_6$] CH$_3$CN solution.
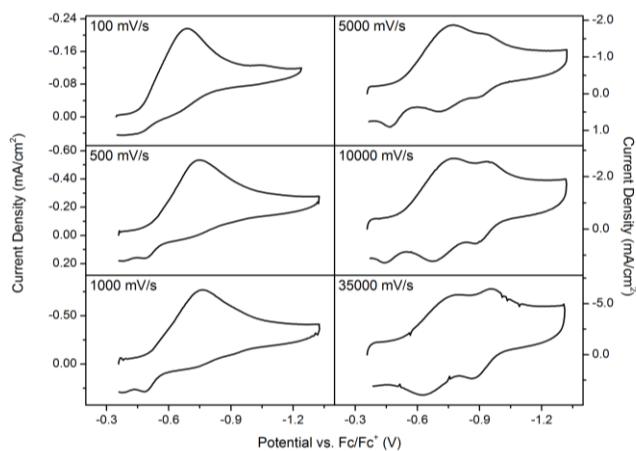

Figure SE3. Cyclic voltammograms of 0.45 mM **2** with one molar equivalent of *p*-toluenesulfonic acid, at varying scan rates. Recorded in 0.25 M [Bu$_4$N][PF$_6$] CH$_3$CN solution.
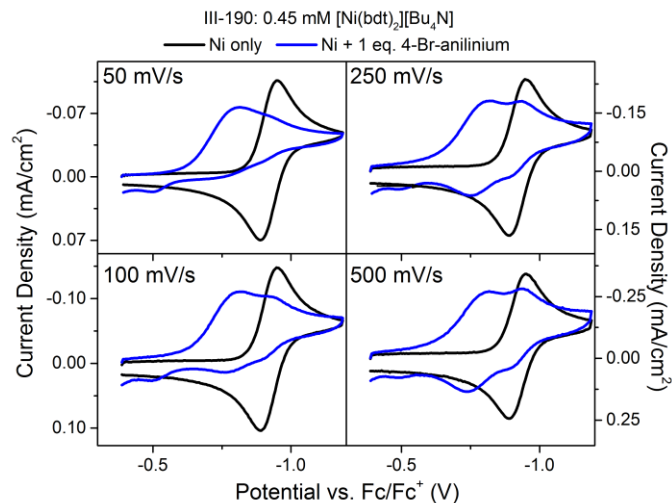
Figure SE4. Cyclic voltammograms of 0.45 mM **2** with and without one molar equivalent of 4-bromoanilinium at various scan rates. Recorded in 0.25 M [Bu$_4$N][PF$_6$] CH$_3$CN solution.
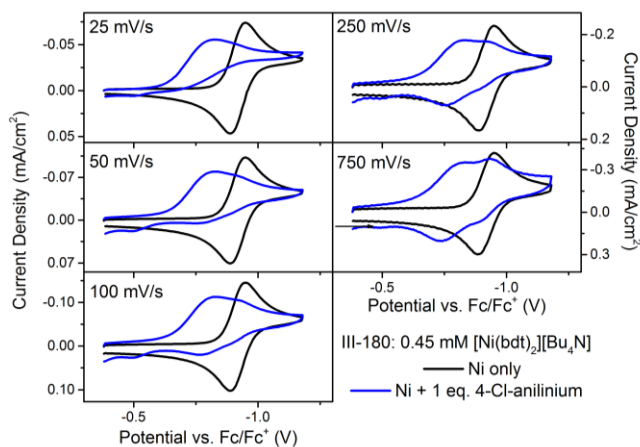

Figure SE5. Cyclic voltammograms of 0.45 mM **2** with and without one molar equivalent of 4-chloroanilinium at various scan rates. Recorded in 0.25 M [Bu$_4$N][PF$_6$] CH$_3$CN solution.
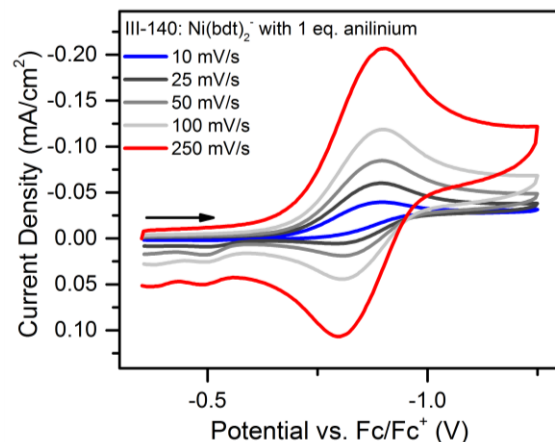
22

Figure SE6. Cyclic voltammograms of 0.45 mM **2** with and without one molar equivalent of anilinium at various scan rates. Recorded in 0.25 M [Bu₄N][PF₆] CH₃CN solution.
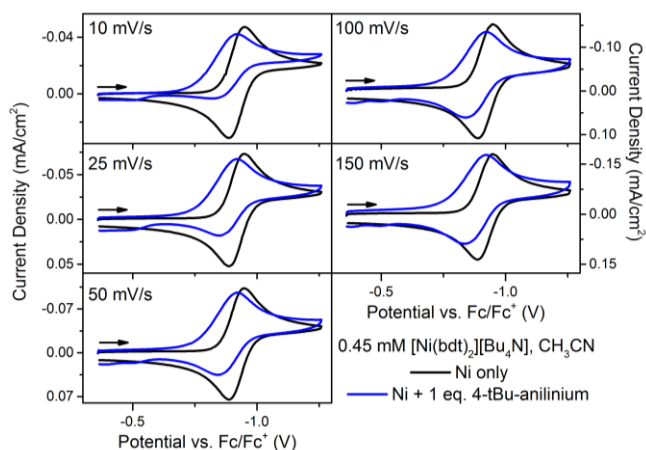

Figure SE7. Cyclic voltammograms of 0.45 mM **2** with and without one molar equivalent of 4-*tert*-butylanilinium at various scan rates. Recorded in 0.25 M [Bu₄N][PF₆] CH₃CN solution.
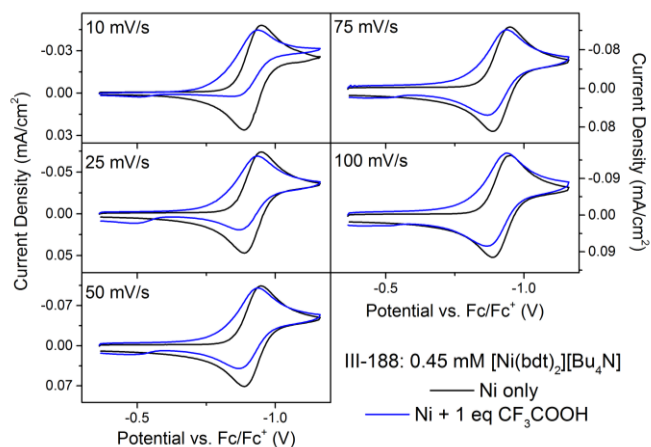

Figure SE8. Cyclic voltammograms of 0.45 mM **2** with and without one molar equivalent of trifluoroacetic acid at various scan rates. Recorded in 0.25 M [Bu₄N][PF₆] CH₃CN solution.
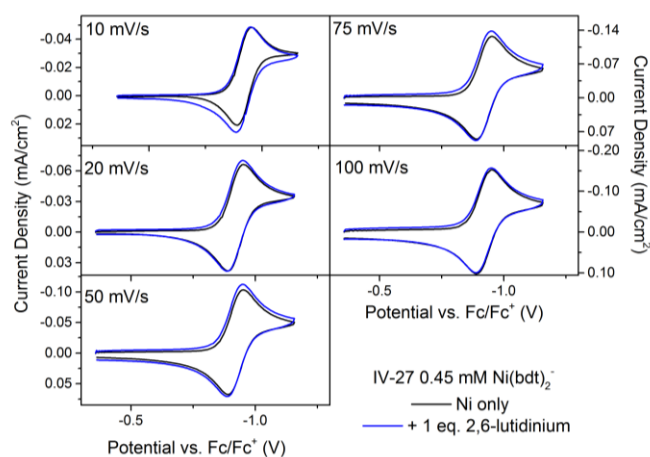
Figure SE9. Cyclic voltammograms of 0.45 mM **2** with and without one molar equivalent of 2,6-lutidinium at various scan rates. Recorded in 0.25 M [Bu$_4$N][PF$_6$] CH$_3$CN solution.
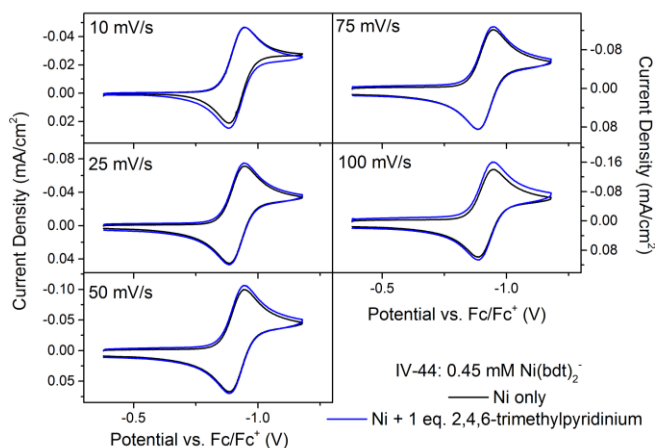

Figure SE10. Cyclic voltammograms of 0.45 mM **2** with and without one molar equivalent of 2,4,6-trimethylpyridinium at various scan rates. Recorded in 0.25 M [Bu$_4$N][PF$_6$] CH$_3$CN solution.
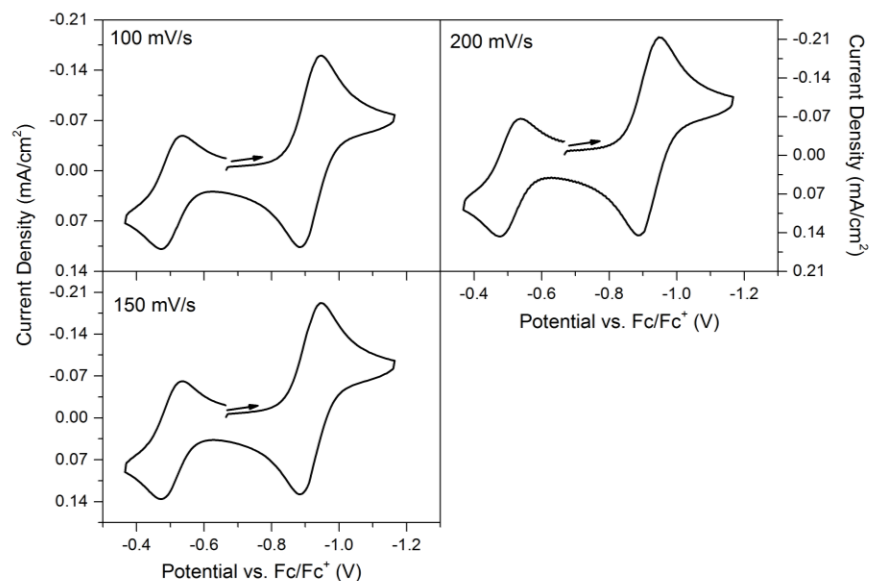
Figure SE11. Cyclic voltammograms of 0.5 mM **2** with one molar equivalent of 4-CF$_3$-2,3,5,6-F$_4$-PhOH at various scan rates. Recorded in 0.25 M [Bu$_4$N][PF$_6$] CH$_3$CN solution.
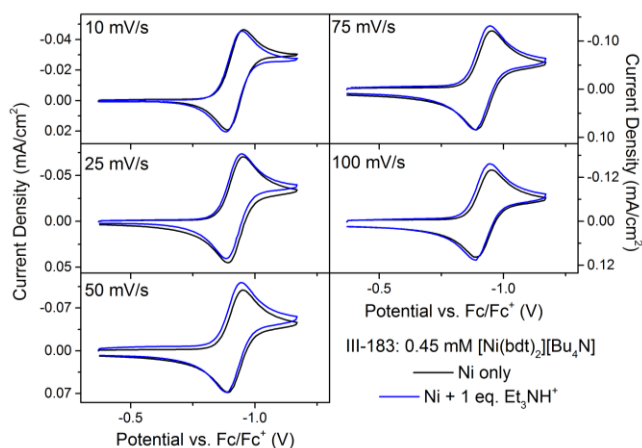

Figure SE12. Cyclic voltammograms of 0.45 mM **2** with and without one molar equivalent of triethylammonium at various scan rates. Recorded in 0.25 M [Bu$_4$N][PF$_6$] CH$_3$CN solution.

F. Non-Nernstian shifts observed for 2 in acid/conjugate base titrations

Case 1: Homoconjugation of acid and conjugate base

The 4-Cl-anilinium/4-Cl-aniline data of Fig. 5 represents an idealized case where individual molecules of acid and conjugate base interact weakly. Many acids aggregate in non-aqueous solvents where solvation is poor (e.g., dimers of carboxylic acids). Additionally, acid (HA) may interact with its conjugate base (A⁻), a process termed homoconjugation:[1,15–17]

$$A^- + HA \rightleftharpoons A^- \cdots HA$$
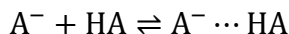
Homoconjugation can have a profound influence – the concentration of non-associated acid is reduced, the acidity of HA may be increased through stabilization of newly generated conjugate base with unreacted parent acid, and the homoconjugated species has a different pK_a.[1]

Substituted anilinium acids generally homoconjugate weakly (the homoconjugation formation constant for anilinium is about 4);[7] consequently, the 4-Cl-anilinium/4-Cl-aniline data in the main text were not expected to show significant deviations from the predicted slope. When the same titration is performed with p-toluenesulfonic acid, which possesses a large homoconjugation constant of about 1000,[7] the plot of $E_{1/2}$ potential plotted versus the inverse log of the tosylate concentration is non-linear (Fig. SF1).

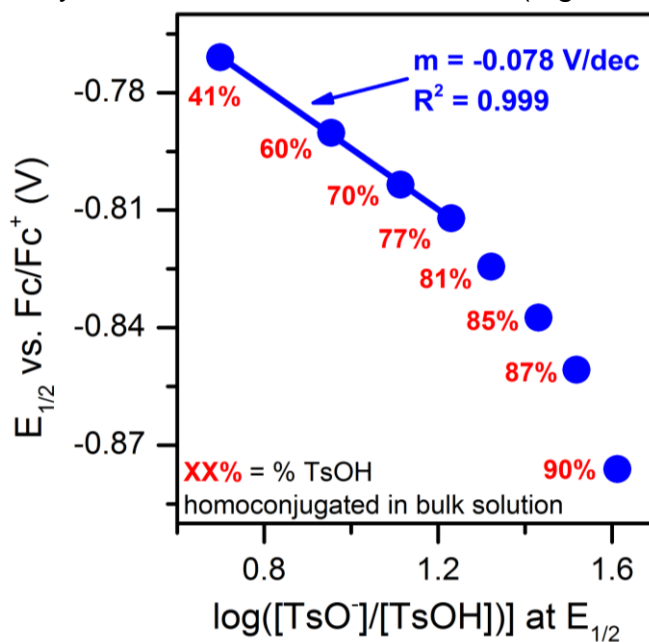**Figure SF1.** Plot of the $E_{1/2}$ value for a solution of 0.45 mM **2** versus the log of varying ratios of tosylate to p-toluenesulfonic acid. Percentage values (in red) next to each data point indicate the percentage of p-toluenesulfonic acid homoconjugated in the bulk solution.

The overall non-linearity of the titration data matches the expected equilibrium of p-toluenesulfonic acid with its homoconjugated form.

This data can be partially corrected (Fig. SF2) by calculating how much non-homoconjugated acid is initially present based on the homoconjugation formation constant and initial concentrations, followed by estimation of the concentrations of tosic acid and tosylate at the $E_{1/2}$ value. The homoconjugation formation constant of p-toluenesulfonic acid is known to be approximately 1000,[7] and so calculations were performed to estimate the amount of p-toluenesulfonic acid existing as free acid, the amount present as the homoconjugated product, and the amount of conjugate base remaining. Using this analysis, the amount of free acid present at the electrode prior to the experiment beginning may be approximated. Fig. SF2 compares the raw data with the data corrected for homoconjugation.
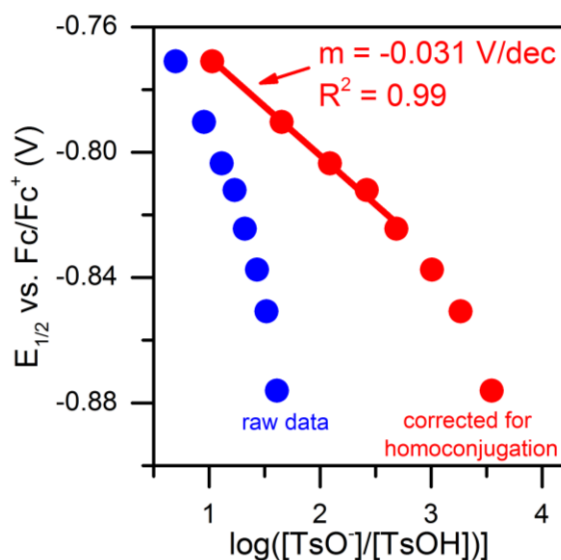

Figure SF2. Blue points are the plot of the $E_{1/2}$ value for each CV titration of tosylate (TsO⁻) versus the calculated log of the ratio of the concentrations of tosylate to p-toluenesulfonic acid at $E_{1/2}$ *assuming no homoconjugation*. Red points show the data corrected for homoconjugation.

As Figure SF2 shows, homoconjugation could not be completely corrected. Multiple factors render this challenging. First, as soon as PCET begins occurring at the electrode surface the relative concentrations of acid, conjugate base, and homoconjugated acid/base pair begin to change rapidly. Second, the homoconjugated acid (of unknown pK_a) may still participate in PCET electrochemistry. Consequently, studies with this sort of analysis should, if possible, strive to utilize acid/base pairs that homoconjugate weakly and to utilize dilute solutions.

Case 2: Competition between PCET and electron transfer

A second example of a non-Nernstian response was seen for titration of aniline to a 1:1 mixture of **2** and anilinium; a slope of 46 mV/decade was observed (Figure SF3). Compared to *p*-toluenesulfonic acid, anilinium and aniline associate much more weakly in acetonitrile.[7] A more plausible explanation is that as the aniline concentration increases, the $E_{1/2}$ shifts close to the original redox couple of **2** in the absence of acid ($E_{1/2}$(**2$^{0/-}$**)) – only 10 equivalents of added base are required to shift the observed $E_{1/2}$ to within 20 mV of $E_{1/2}$(**2$^{0/-}$**). As detailed for **1**, and also seen in the potential-pK_a diagram of **2**, curvature is observed between the linear PCET region and the pK_a-independent region. For anilinium, addition of aniline shifts the redox potential into the curved region. 4-chloroanilinium exhibits Nernstian behavior because it both homoconjugates weakly and because the PCET redox wave without added base is over 100 mV positive of $E_{1/2}$(**2$^{0/-}$**).
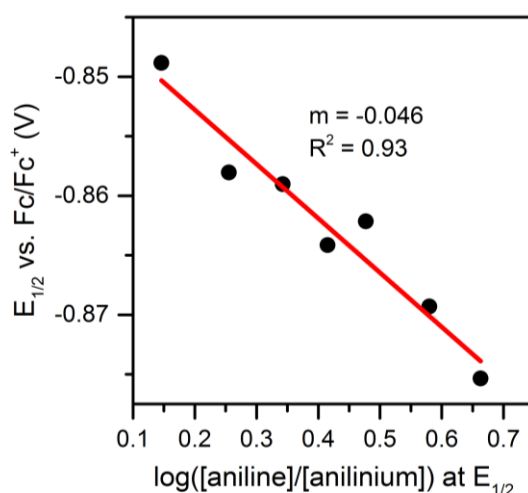

Figure SF3. Plot of the $E_{1/2}$ value for a solution of 0.45 mM **2** versus the log of varying ratios of aniline to anilinium in solution.

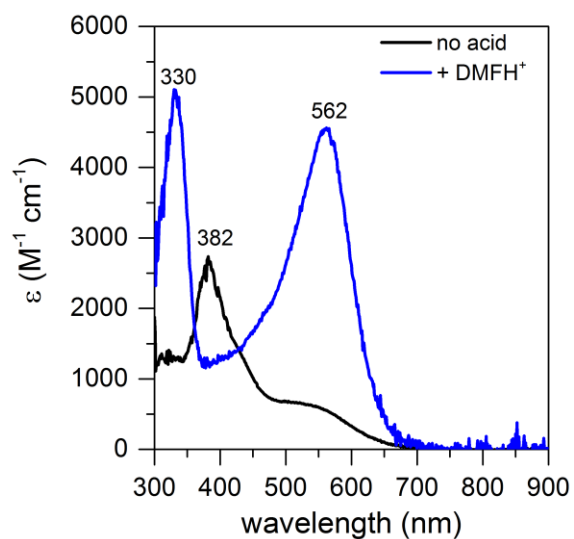## G. UV-vis absorbance spectra of compound 1

Figure SG1. Extinction coefficients of compound **1** in acetonitrile without acid (black) and with 5.2 equiv. of dimethylformamidium triflate (blue).

H. References

(1)   McCarthy, B. D.; Martin, D. J.; Rountree, E. S.; Ullman, A. C.; Dempsey, J. L. *Inorg. Chem.* **2014**, *53*, 8350.

(2)   Rountree, E. S.; Martin, D. J.; McCarthy, B. D.; Dempsey, J. L. *ACS Catal.* **2016**, *6*, 3326.

(3)   McCarthy, B. D.; Donley, C. L.; Dempsey, J. L. *Chem. Sci.* **2015**, *6*, 2827.

(4)   Baker-Hawkes, M. J.; Billig, E.; Gray, H. B. *J. Am. Chem. Soc.* **1966**, *88*, 4870.

(5)   Whalley, A. L.; Blake, A. J.; Collison, D.; Davies, E. S.; Disley, H. J.; Helliwell, M.; Mabbs, F. E.; McMaster, J.; Wilson, C.; Garner, C. D. *Dalt. Trans.* **2011**, *40*, 10457.

(6)   Fulmer, G. R.; Miller, A. J. M.; Sherden, N. H.; Gottlieb, H. E.; Nudelman, A.; Stoltz, B. M.; Bercaw, J. E.; Goldberg, K. I. *Organometallics* **2010**, *29*, 2176.

(7)   Izutsu, K. *Acid-Base Dissociation Constants in Dipolar Aprotic Solvents; IUPAC Chemical Data Series*; Blackwell Scientific Publications: Oxford, UK, 1990.

(8)   Appel, A. M.; Lee, S.; Franz, J. A.; DuBois, D. L.; Rakowski DuBois, M.; Twamley, B. *Organometallics* **2009**, *28*, 749.

(9)   Kaljurand, I.; Kütt, A.; Sooväli, L.; Rodima, T.; Mäemets, V.; Leito, I.; Koppel, I. A. *J. Org. Chem.* **2005**, *70*, 1019.

(10) Kütt, A.; Leito, I.; Kaljurand, I.; Sooväli, L.; Vlasov, V. M.; Yagupolskii, L. M.; Koppel, I. A. *J. Org. Chem.* **2006**, *71*, 2829.

(11) Rountree, E. S.; Dempsey, J. L. *Inorg. Chem.* **2016**, *55*, 5079.

(12) Savéant, J.-M. *Elements of Molecular and Biomolecular Electrochemistry*; John Wiley & Sons, Inc.: Hoboken, 2006.

(13) Warren, J. J.; Tronic, T. A; Mayer, J. M. *Chem. Rev.* **2010**, *110*, 6961.

(14) Nicholson, R. S.; Shain, I. *Anal. Chem.* **1964**, *36*, 706.

(15) Coetzee, J. F. In *Progress in Physical Organic Chemistry: Volume 4*; Streitwieser Jr., A., Taft, R. W., Eds.; John Wiley & Sons, Inc.: Hoboken, NJ, 1967; pp 45–92.

(16) French, C. M.; Roe, I. G. *Trans. Faraday Soc.* **1953**, *49*, 314.

(17) Fourmond, V.; Jacques, P.-A.; Fontecave, M.; Artero, V. *Inorg. Chem.* **2010**, *49*, 10338.